

Earth's Future

L

RESEARCH ARTICLE

10.1029/2021EF002351

Special Section:

Atmospheric Rivers: Intersection of Weather and Climate

Key Points:

- Ural Blocking plays an important role in the occurrence of the sub-seasonal warm Arctic-cold Eurasia (WACE) dipole pattern in winter
- Ural blocking can amplify the wintermean Warm Arctic-cold Eurasia (WACE) pattern
- Warm Arctic-cold Eurasia (WACE) is linked to the Pacific Decadal Oscillation (PDO) and Atlantic Multidecadal Oscillation (AMO)

Correspondence to:

D. Luo, ldh@mail.iap.ac.cn

Citation:

Luo, B., Luo, D., Dai, A., Simmonds, I., & Wu, L. (2022). Decadal variability of winter warm Arctic-cold Eurasia dipole patterns modulated by Pacific Decadal Oscillation and Atlantic Multidecadal Oscillation. *Earth's Future*, 10, e2021EF002351. https://doi.org/10.1029/2021EF002351

Received 19 AUG 2021 Accepted 20 DEC 2021

Author Contributions:

Conceptualization: Binhe Luo, Dehai Luo

Luo

Data curation: Binhe Luo Formal analysis: Binhe Luo Methodology: Binhe Luo, Dehai Luo Supervision: Dehai Luo Visualization: Binhe Luo

Writing – original draft: Binhe Luo,

Dehai Luo, Aiguo Dai

Writing – review & editing: Binhe Luo, Dehai Luo, Aiguo Dai, Ian Simmonds, Lixin Wu

© 2021 The Authors. Earth's Future published by Wiley Periodicals LLC on behalf of American Geophysical Union. This is an open access article under the terms of the Creative Commons Attribution License, which permits use, distribution and reproduction in any medium, provided the original work is properly cited.

Decadal Variability of Winter Warm Arctic-Cold Eurasia Dipole Patterns Modulated by Pacific Decadal Oscillation and Atlantic Multidecadal Oscillation

Binhe Luo^{1,2}, Dehai Luo², Aiguo Dai³, Ian Simmonds⁴, and Lixin Wu¹

¹Key Laboratory of Physical Oceanography/Institute for Advanced Ocean Studies, Ocean University of China and Qingdao National Laboratory for Marine Science and Technology, Qingdao, China, ²Key Laboratory of Regional Climate-Environment for Temperate East Asia, Institute of Atmospheric Physics, Chinese Academy of Sciences, University of Chinese Academy of Sciences, Beijing, China, ³Department of Atmospheric and Environmental Sciences, University at Albany, Albany, NY, USA, ⁴School of Geography, Earth and Atmospheric Sciences, University of Melbourne, Melbourne, VIC, Australia

Abstract In recent decades, the winter surface air temperature (SAT) anomaly in the Northern Hemisphere has exhibited a warm Arctic-cold Eurasia (WACE) dipole pattern and this has undergone significant decadal variation. In this paper, the physical cause of the decadal variability of the WACE pattern is explored, and it is shown to be mediated by the phases of the Pacific Decadal Oscillation (PDO) and Atlantic Multidecadal Oscillation (AMO). Although the negative PDO (PDO⁻) or positive AMO (AMO⁺) favors the WACE pattern, the meridional structure of the pattern is significantly influenced by whether PDO⁻ or AMO⁺ dominates. During PDO⁻ (AMO⁺) phase, the winter-mean WACE pattern shows an asymmetric dipole with weak (strong) warm anomaly over the Barents-Kara Seas or BKS and strong (weak) cold anomaly over central Eurasia or Siberia, which corresponds to Ural blocking (UB) concurring with the negative (positive) phase of North Atlantic Oscillation in a winter-mean field. The winter asymmetric WACE pattern is more strongly related to PDO⁻ than AMO⁺. It is further found that an asymmetric sub-seasonal WACE dipole pattern with strong (weak) warm anomaly over BKS and weak (strong) cold anomaly over Siberia is usually formed during the UB episode due to favored (suppressed) sub-seasonal downward infrared radiation and turbulent heat flux over BKS during AMO⁺ (PDO⁻), which leads to a strong asymmetric dipole of the winter WACE pattern.

Plain Language Summary The most prominent climate change in the Northern Hemispheric mid-high latitudes in recent decades is that the winter surface air temperature anomaly has exhibited a warm Arctic-cold Eurasia (WACE) dipole pattern. However, it is still unknown what causes the decadal variability of the winter WACE pattern and its meridional asymmetry. In this paper, we address this issue by examining the different effects of Pacific Decadal Oscillation (PDO) and Atlantic Multidecadal Oscillation (AMO) on the winter WACE pattern. It is shown that PDO⁻ (AMO⁺) plays an important role in the occurrence of the asymmetric WACE dipole with weak (strong) warm anomaly over the Barents-Kara Seas and strong (weak) cold anomaly over central Eurasia or Siberia through modulating Ural blocking and associated sub-seasonal cold anomaly. It is also found that the asymmetric WACE dipole is more strongly dependent on PDO⁻ than AMO⁺. Our findings are of great significance for understanding the physical cause of the decadal variability of the WACE dipole pattern in spatial structure.

1. Introduction

A prominent feature of Northern Hemisphere (NH) climate variations in recent decades is the warm Arctic-cold Eurasia (WACE) pattern in winter surface air temperature (SAT) (Cohen et al., 2014; Kim & Son, 2016; Kug et al., 2015; Mori et al., 2014; Overland et al., 2011; Shepherd, 2016). In recent years, the physical cause of the generation and variability of the Eurasian cold anomaly or WACE dipole pattern has attracted considerable attention and has been an important research topic (Chen et al., 2021; Deser et al., 2017; Jin et al., 2020; Kim et al., 2021; Li et al., 2015; B. Luo et al., 2019; McCusker et al., 2016; Overland et al., 2015; Sun et al., 2016; Sung et al., 2018; Wegmann et al., 2018; Xu et al., 2018; Yao et al., 2017; Ye & Messori, 2020).

The WACE pattern varies on a broad range of timescales, including sub-seasonal (10-20 days) (Kim et al., 2021; Luo, Xiao, Diao, et al., 2016; Luo, Xiao, Yao, et al., 2016; Tyrlis et al., 2020), interannual, and decadal-interdecadal

LUO ET AL.

Earth's Future 10.1029/2021EF002351

periods (Chen et al., 2021; Jin et al., 2020; D. Luo et al., 2017; Luo et al., 2021; Sung et al., 2018). On decadal-interdecadal timescales, the Atlantic Multidecadal Oscillation (AMO) and the Pacific Decadal Oscillation (PDO) are two prominent modes of SST variability in the North Atlantic with a period of 60-80 years (Trenberth and Shea, 2006) and in the North Pacific with a period of 20-30 years (Mantua et al., 1997). Previous studies have indicated that winter SAT in the Arctic and NH is modulated by AMO (Chylek et al., 2009; Wyatt et al., 2012), and the interdecadal variations in winter Eurasian cold anomaly or the WACE pattern are associated with sea surface temperature (SST) anomalies over the North Atlantic (Chen et al., 2021; Jin et al., 2020; D. Luo et al., 2017; Sung et al., 2018) and Pacific (Dai et al., 2015; Huang et al., 2017).

Ural blocking (UB) is a quasi-stationary anticyclonic anomaly circulation occurring over the Ural Mountains and adjacent regions with a sub-seasonal timescale of 10-20 days. It has been recognized that the presence of UB can lead to a strong sub-seasonal WACE pattern (Kim et al., 2021; Luo et al., 2021; B. Luo et al., 2019; D. Luo et al., 2019; D. Luo et al., 2017; Luo, Xiao, Diao, et al., 2016; Luo, Xiao, Yao, et al., 2016; Tyrlis et al., 2020; Yao et al., 2017; Ye & Messori. 2020), and most of the UB events are related to the decay of the positive North Atlantic Oscillation (NAO) with a meridional dipole (Luo, Xiao, Diao, et al., 2016). To a large extent, the winter-mean WACE pattern is an averaged result of the winter sub-seasonal WACE patterns (Kim et al., 2021; Luo, Xiao, Diao, et al., 2016; Luo, Xiao, Yao, et al., 2016; Tyrlis et al., 2020). Because PDO and AMO occur on decadal timescales, it might be inferred that the PDO and AMO can induce decadal variations of the winter WACE pattern through their modulation of the sub-seasonal WACE patterns, whereas the interannual variability of the winter WACE pattern is modulated by El Niño-Southern Oscillation (ENSO) (Luo et al., 2021). Recently, D. Luo et al. (2017), Sung et al. (2018) and Jin et al. (2020) have examined AMO's impact on the winter WACE pattern on interdecadal timescales and found that the phase of AMO can modulate the winter WACE pattern through a change in sea ice over the Barents-Kara Seas (BKS) and atmospheric wave propagation from the North Atlantic to Eurasia. Dai et al. (2015) also noted that the WACE pattern is linked to the negative phase of the Interdecadal Pacific Oscillation (Power et al., 1999) or PDO, but they did not present the connection mechanism. Because PDO modulates the stratospheric Arctic vortex (Hu and Guan, 2018) and AMO affects sea ice variability over the BKS (D. Luo et al., 2017), they may influence the meridional structure of the winter WACE pattern through the variability of UB and associated sub-seasonal SAT anomalies. However, it is unclear whether the winter SST anomalies over the North Atlantic and Pacific have different contributions to the meridional structure of the WACE dipole pattern on decadal to interdecadal timescales, and what role UB may play in this connection.

In this paper we will examine the different effects of PDO and AMO on the variability of the WACE dipole pattern by analyzing 70 years of observational and reanalysis data because they are the leading SST modes on decadal-interdecadal timescales over the Pacific and North Atlantic (Dong and Dai, 2015; Qin et al., 2020). We will be particularly interested in exposing the roles that negative PDO and positive AMO phases separately play in determining the meridional structure of the WACE pattern on decadal timescales, and how these influences are realized by the UB occurrence.

2. Data and Method

We used the monthly- and daily-mean data on a $1^{\circ} \times 1^{\circ}$ grid for winter (December, January and February; DJF) during the period from December 1950/February 1951 to December 2019/February 2020 (1950–2019 hereafter) from the ERA5 reanalysis data from European Centre for Medium Range Weather Forecasts (Hersbach et al., 2020; https://climate.copernicus.eu/climate-reanalysis). The daily data include 500-hPa geopotential height (Z500), surface air temperature (SAT), total column water vapor, downward infrared radiation (IR), and surface sensible and latent heat fluxes. The monthly SST data were taken from the Hadley Centre SST (HadISST) dataset on $1^{\circ} \times 1^{\circ}$ grid during December 1950/February 1951–December 2019/February 2020 (1950–2019) (Rayner et al., 2003; https://www.metoffice.gov.uk/hadobs/index.html). The long-term (1950–2019) mean and linear trend of all the daily or monthly data for each calendar day or month are removed to generate de-seasonalized anomaly data.

In this paper, we use the 9-year low pass filtered normalized time series of the principal components (PCs) of leading empirical orthogonal function (EOF) modes of the DJF-mean SST anomaly fields (from HadISST, with the linear trend removed) over the North Pacific (120°E–90°W, 10°–60°N) and North Atlantic (80°W–0°, 20°–70°N) to reflect the decadal and interdecadal variations of the winter SST anomalies over North Pacific and

LUO ET AL. 2 of 14

North Atlantic respectively. As indicated by Wang and An (2005), the seasonal-mean EOF analysis can efficiently detect major modes of winter climate variability, which is the focus of this study. Thus, here we perform the EOF analysis of DJF-mean SST anomalies over the North Pacific and North Atlantic, rather than directly using the conventional PDO and AMO indices that often include all months.

Our calculation reveals that the correlation coefficients of the normalized SST PC1 time series over the North Pacific and North Atlantic with the winter PDO and AMO indices taken from the Koninklijk Nederlands Meteorologisch Instituut (KNMI) Climate Explorer (http://climexp.knmi.nl/selectindex.cgi?id=someone@somewhere) are 0.93 and 0.85, respectively. Thus, the 9-year low-pass filtered DJF-mean SST EOF1 mode over the North Pacific (North Atlantic) can approximately represent the winter PDO (AMO) SST patterns on decadal timescales. In the present study, the EOF analysis of the Pacific SST anomaly is performed in the North Pacific (Liu and Lorenzo, 2018). It is noted that a slightly different choice of the EOF domain does not change our results (not shown). Our calculations also indicate that the results obtained in this paper are insensitive to the different indices of PDO (Dong and Dai, 2015; Power et al., 1999) and AMO (Dai, 2013; Enfield et al., 2001; Sutton and Dong, 2012; Trenberth and Shea, 2006) (not shown).

The daily NAO index from the NOAA Climate Prediction Center (CPC) (https://www.cpc.ncep.noaa.gov/products/precip/CWlink/pna/nao.shtml) is used to define individual NAO events. We also define a NAO+ (NAO-) event to have taken place if the daily NAO index is above 0.5 (below –0.5) standard deviations (STDs) and persists for at least three consecutive days. All other NAO events are defined as neutral NAO (NAO-) events. The life cycle of the NAO+ (NAO-) is defined to begin when the daily index starts from a zero value, continues to its peak of the positive (negative) daily NAO index, and then declines (increases) to the day with a zero value again when the event is considered to end.

To identify UB events in the Ural Mountains region 40° - 80° E, we used the one-dimensional blocking index of Tibaldi and Molteni (1990), TM hereafter. The TM index is based on the reversal of the meridional Z500 gradient: GHGN = $[Z500(\phi_N) - Z500(\phi_o)]/(\phi_N - \phi_o)$ and GHGS = $[Z500(\phi_o) - Z500(\phi_S)]/(\phi_o - \phi_S)$ at three given latitudes $\phi_N = 80^{\circ}N + \Delta$, $\phi_o = 60^{\circ}N + \Delta$, $\phi_S = 40^{\circ}N + \Delta$ and $\Delta = -5^{\circ}$, 0° , 5° . A blocking event is defined to have taken place if the conditions GHGS > 0 and GHGN < -10 gpm (deg lat)⁻¹ hold for at least three consecutive days and are satisfied for at least one choice of Δ in a given zonal region covering at least 15 longitudes. We refer to the UB as being related to an NAO+(NAO-) event if the peak day of the GHGS occurs within the life cycle of an NAO+(NAO-) event (as in B. Luo et al. (2017)) and denote such an occurrence as a UB-NAO+(UB-NAO-) event. Similarly, when a UB is related to a NAO° occurrence, it is referred to as the UB-NAO° event.

To reflect the variation of the winter WACE dipole pattern, we define the difference of the domain-averaged DJF-mean SAT anomaly between the Barents-Kara Seas (30°-90°E, 65°-85°N; BKS) and central Eurasia (60°-120°E, 40°-60°N; CE) or Siberia as a winter WACE index. Moreover, we used a two-sided student t-test to examine the statistical significance of the anomaly fields in this paper. The statistical significance test of the correlation between various time series is performed using a student t-test. These statistical methods can be found in Wilks (2011).

3. Results

We first show the time series of the normalized DJF-mean WACE index during 1950–2019 in Figure 1a. The WACE index shows substantial decadal variability (Figure 1a), and is mostly positive during three sub-periods (1950–1956, 1966–1976 and 2004–2019), and predominantly negative during two sub-periods (1957–1965 and 1977–2003). These decadal variations are suggestive of links to the low-frequency PDO and AMO, as noted below. To reveal the role of UB in the winter WACE pattern via the variability of the sub-seasonal WACE patterns, we show the DJF-mean fields of composite daily Z500 and SAT anomalies with and without UB events for a positive WACE (WACE+) index winters (19 cases) with ≥0.5 STDs of the 9-year low-pass filtered WACE index and their difference field in Figures 1b and 1c. It is found that there are 36 UB events in the 19 WACE+ winters. Here, the winter average of daily Z500 and SAT anomalies with the removal of all the blocking days of 36 UB events (blocking days from lag −10 to 10 are removed, where lag 0 denotes the peak day of UB) is defined as the winter WACE pattern without UB events. Clearly, the WACE pattern is very weak in the absence of UB events (Figure 1c), but strong for UB events included (Figure 1b). The difference of the composite DJF-mean Z500 and SAT anomalies between the two cases with and without UB events (Figure 1d) suggests that UB can have a large

LUO ET AL. 3 of 14

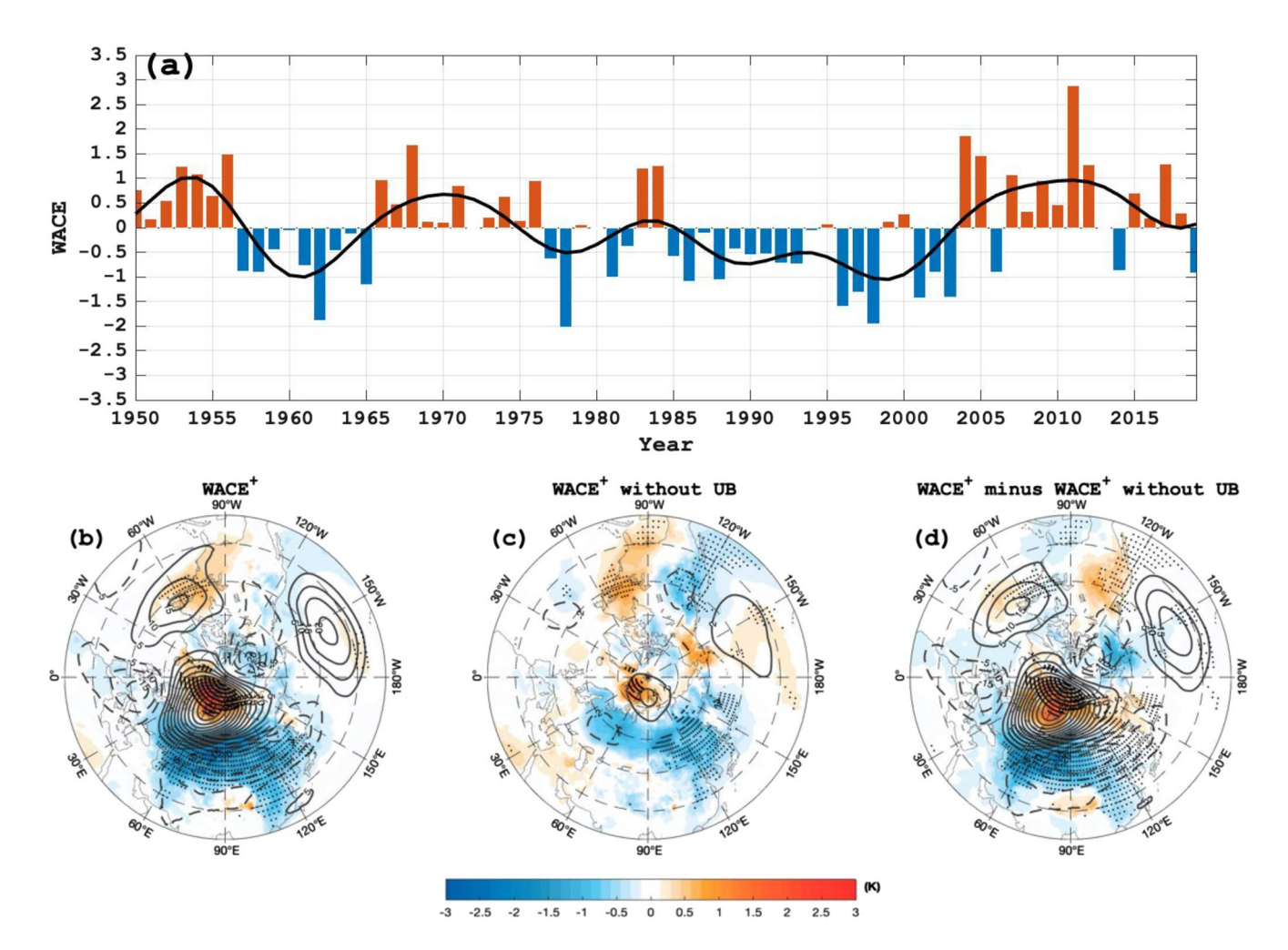


Figure 1. (a) Time series of winter warm Arctic-cold Eurasia (WACE) index, defined as the difference of the December, January and February (DJF)-mean surface air temperature (SAT) anomaly between the Barents-Kara Seas $(30^{\circ}-90^{\circ}\text{E}, 65^{\circ}-85^{\circ}\text{N})$ and central Eurasia $(60^{\circ}-120^{\circ}\text{E}, 40^{\circ}-60^{\circ}\text{N}; CE)$. (b and c) Composite DJF-mean Z500 (contours, contour interval (CI) = 5 gpm) and SAT (color shading, in K) anomalies for a positive WACE (WACE+) index with ≥ 0.5 STDs in panel b with and panel c without UB events and panel d their difference field. The dot represents the shading region with a 95% confidence level based on a two-sided student t-test. The thick line denotes a 9-yr low pass curve.

contribution to the winter WACE pattern through generating sub-seasonal WACE events. In other words, most of the winter WACE pattern can be characterized by a winter average of sub-seasonal WACE patterns. Thus, the decadal variability of the winter WACE pattern is likely attributed to decadal changes in the sub-seasonal WACE patterns modulated by PDO and AMO. Because the linkage of the winter WACE pattern to sub-seasonal WACE patterns associated with UB events or with the different phase of NAO has been established in Luo, Xiao, Diao, et al. (2016); Luo, Xiao, Yao, et al. (2016), below we do not repeat this discussion on the linkage between the two timescales. Instead, our emphasis is focused on the modulation of PDO and AMO on the sub-seasonal and winter WACE patterns.

It is also useful to show the time series of the normalized domain-averaged DJF-mean SAT anomalies over BKS and CE separately during 1950–2019 in Figures 2a and 2b. The winter BKS SAT time series has a negative correlation of –0.02 (–0.24) with the CE SAT time series for the case without (with) a 9-year low pass filtered smoothing, suggesting that the CE SAT anomaly could be linked to the BKS SAT anomaly on decadal time-scales. M. Li et al. (2021) and Rudeva and Simmonds (2021) have shown a strong interannual inverse connection between conditions in the BKS and China. The regressed DJF-mean Z500 and SAT anomalies onto the 9-year low pass filtered normalized DJF-mean BKS and CE SAT time series are shown in Figures 2c and 2d. These regression maps make it clear that the DJF-mean warm anomaly over BKS corresponds to a combination of the UB and NAO+ patterns (Figure 2c), whereas the cold anomaly over CE is related to the combined UB and NAO- pattern similar

LUO ET AL. 4 of 14

23284277, 2022. 1, Downloaded from https://gupubs.onlinelibrary.wiley.com/doi/10.1029/2021EF002351 by Suny University At Albany, Wiley Online Library on [02/06/203]. See the Terms and Conditions (https://onlinelibrary.wiley.com/doi/10.1029/2021EF002351 by Suny University At Albany, Wiley Online Library on [02/06/203]. See the Terms and Conditions (https://onlinelibrary.wiley.com/doi/10.1029/2021EF002351 by Suny University At Albany, Wiley Online Library on [02/06/203]. See the Terms and Conditions (https://onlinelibrary.wiley.com/doi/10.1029/2021EF002351 by Suny University At Albany, Wiley Online Library on [02/06/203]. See the Terms and Conditions (https://onlinelibrary.wiley.com/doi/10.1029/2021EF002351 by Suny University At Albany, Wiley Online Library on [02/06/203].

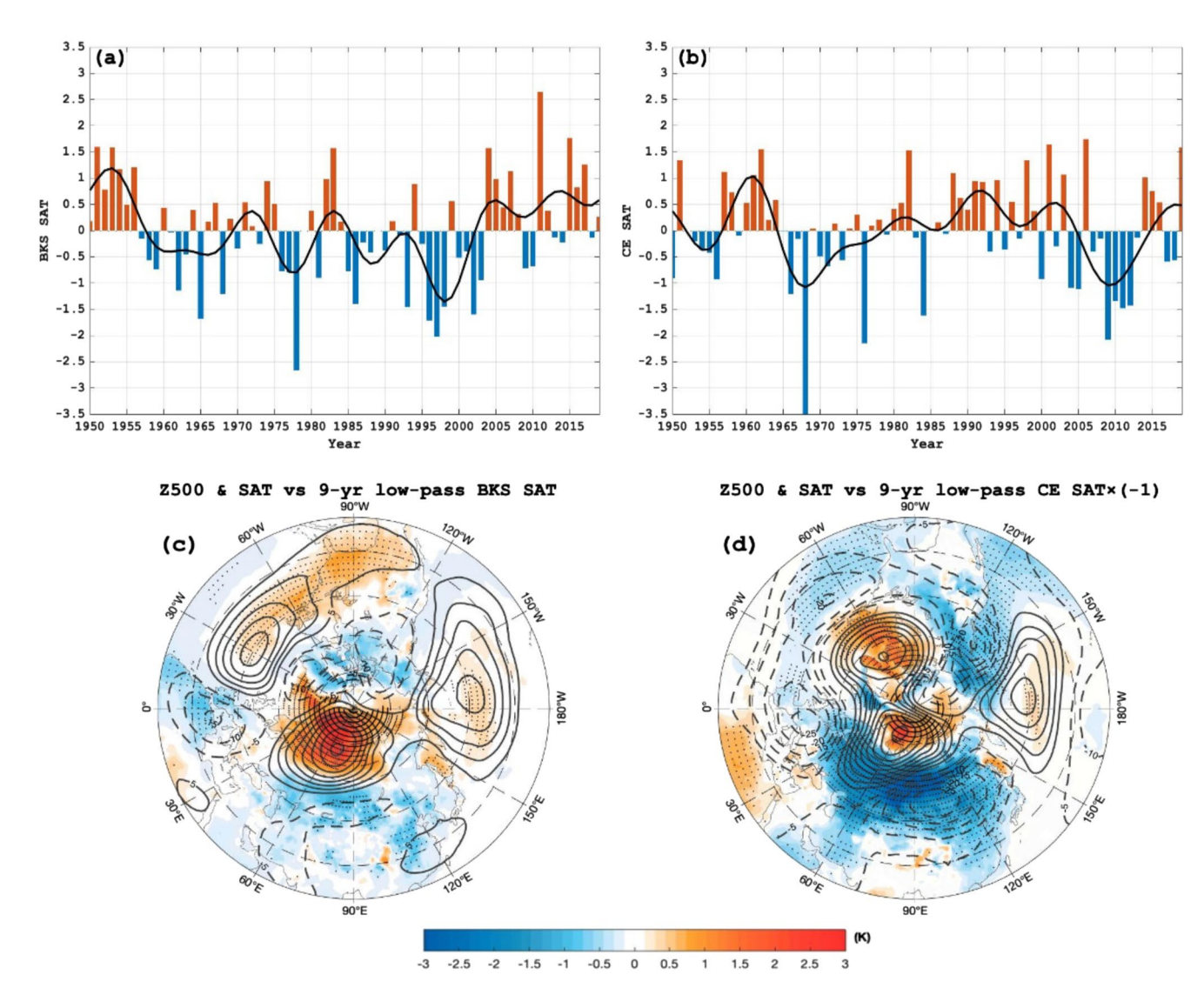


Figure 2. (a and b) Normalized time series of December, January and February (DJF)-mean SAT anomalies averaged over (a) BKS and (b) CE. (c, d) Regressed DJF-mean Z500 (contours, CI = 5 gpm STD⁻¹) and SAT (color shading, in K) anomalies onto the 9-yr low pass filtered domain-averaged SAT time series over (c) BKS and (d) CE. The dot represents the shading region with a 95% confidence level based on a two-sided student t-test. The thick line denotes a 9-yr low pass curve.

to a negative Arctic Oscillation (AO⁻) (Figure 2d). As noted by Luo, Xiao, Diao, et al. (2016), the winter Z500 and SAT anomaly patterns can be mostly reflected by the winter average of UB events and associated sub-seasonal SAT anomalies, as also seen from Figures 1b and 1d. Thus, it is useful to examine the different contributions of UB events under the different phases of NAO to the sub-seasonal SAT anomaly in the following discussions.

As found by B. Luo et al. (2017) and Zhong et al. (2018) from daily and DJF-mean perspectives, the intrusion of North Atlantic midlatitude moisture into BKS is favored (suppressed) when UB occurs together with the NAO+ (NAO-). Such an enhanced (weakened) moisture intrusion into BKS tends to strengthen (reduce) warming or warm SAT anomalies over BKS by enhancing (reducing) downward longwave radiation (see Lee et al., 2017). This explains why a strong (weak) winter warm anomaly mainly occurs over BKS for the UB pattern with NAO+ (NAO-) (Figures 2c and 2d). On the other hand, we find that the strong warm anomaly over BKS does not correspond to a strong cold anomaly over CE (Figure 2c) and vice versa (Figure 2d). Below, we show that such a strong meridional asymmetry of the winter WACE pattern is mainly related to the north-south asymmetries of sub-seasonal WACE patterns associated with UB events occurring together with the different phase of NAO modulated by PDO- and AMO+.

LUO ET AL. 5 of 14

3.1. Meridional Asymmetry of the Winter WACE Dipole Pattern and Its Modulation by PDO and AMO

Before examining the modulation of PDO and AMO on the sub-seasonal WACE patterns associated with UB events, we should first explore whether PDO and AMO modulate the meridional asymmetry of the winter WACE pattern. We show the spatial patterns of the first empirical orthogonal function (EOF1) modes of DJF-mean SST anomalies over North Pacific (120°E-90°W, 10°-60°N) and North Atlantic (80°W-0°, 20°-70°N) and their corresponding normalized PC1 time series in Figures 3a, 3b, 3d, and 3e. The DJF-mean Z500 and SAT anomalies regressed onto the 9-year low pass normalized North Pacific and North Atlantic SST PC1 time series are given in Figures 3c and 3f. It is noted that the SST EOF1 mode explains the 28% (25%) variance of the DJF-mean Pacific (Atlantic) SST anomaly (Figures 3a and 3d), which can reflect the decadal timescale of PDO (AMO) when a 9-year low pass filter is applied to the Pacific (Atlantic) SST PC1 time series (Figures 3b and 3e) because the Pacific (Atlantic) SST PC1 time series has a significant positive correlation of 0.93 (0.85) (p < 0.01) with the winter PDO (AMO) index taken from the KNMI Climate Explorer as noted above. Based on the spatial pattern of the SST EOF1 mode, the negative value of the 9-year low pass filtered normalized Pacific SST PC1 time series corresponds to a negative SST anomaly in the eastern equatorial Pacific and a warm horseshoe pattern in the western or central North Pacific on decadal timescales and thus is defined as the negative phase of the Pacific SST EOF1 mode or the negative Pacific SST EOF1 mode resembling a PDO-. Similarly, the positive value of 9-year low-pass filtered normalized Atlantic SST PC1 time series corresponds to a basin-scale warming over the North Atlantic on decadal timescales and thus is defined as the positive phase of Atlantic SST EOF1 mode or the positive Atlantic SST EOF1 mode, which resembles an AMO+. Clearly, the negative Pacific SST EOF1 mode or PDO- corresponds to a UB with NAO- and a strong asymmetric WACE pattern with a weak warm anomaly over BKS and a strong cold anomaly over CE (Figure 3c). A strong asymmetric WACE pattern with an opposite meridional dipole structure is also seen for the positive Atlantic SST EOF1 mode or AMO+ (Figure 3f). Because the negative Pacific and positive Atlantic SST EOF1 modes can better reflect the PDO- and AMO+ respectively, they can be referred to as the PDO⁻ and AMO⁺ modes hereafter. Thus, a comparison with Figure 2 suggests that AMO+ favors a strong warm/weak cold dipole structure of the WACE pattern, but an opposite meridional asymmetry of the WACE dipole pattern is favored by PDO-.

To further evaluate the dependence of the meridional asymmetry of the winter WACE pattern on PDO and AMO, we show scatter plots of the winter WACE index, BKS and CE SAT time series against the 9-year low-pass normalized Pacific or Atlantic PC1 time series in Figure 4. It is interesting to see that the positive WACE index is favored by PDO⁺ (AMO⁺), but suppressed by PDO⁺ (AMO⁻) (Figures 4a and 4b). Figures 4c and 4f show that the CE SAT anomaly of the winter WACE pattern is mainly determined by the phase of PDO (Figure 4e) rather than by the phase of AMO (Figure 4f), even though its BKS SAT anomaly mainly depends on the phase of AMO (Figure 4d) rather than on the phase of PDO (Figure 4c). We also see that there is a strong CE cold anomaly for PDO⁻ (Figure 4e), but a strong BKS warm anomaly for AMO⁺ (Figure 4d). Thus, the cold (warm) pole of the WACE pattern is more significantly related to PDO⁻ (AMO⁺) than its warm (cold) pole, as also revealed from their correlations in the scatter diagrams in Figure 4. In other words, PDO⁻ (AMO⁺) tends to favor a strong cold (warm) anomaly over CE (BKS). Such an effect leads to an asymmetric WACE dipole pattern during the PDO⁻ (AMO⁺) winter. Moreover, it is noted that the asymmetric WACE dipole pattern is more strongly related to PDO⁻ than AMO⁺ (Figures 4a and 4b) in that the cold SAT anomaly is strong (weak) over CE for PDO⁻ (AMO⁺).

Hu and Guan (2018) found that a weakened stratospheric Arctic vortex is observed during PDO⁻. A weakened vortex results in a NAO⁻ or AO⁻ in the troposphere via the downward propagation of stratospheric planetary waves (Baldwin and Dunkerton, 2001; Lu et al., 2021). As a result, an asymmetric WACE pattern with weak warm/strong cold dipole is inevitably seen via the stratospheric influence during the PDO⁻ winter. In contrast, AMO⁺ tends to strengthen warming over BKS to establish a strong warm/weak cold WACE dipole due to strong sea ice decline over BKS (D. Luo et al., 2017; Simmonds and Li, 2021) via the intrusion of Atlantic warm water into BKS (Årthun et al., 2012) and increased water vapor over BKS (B. Luo et al., 2017). Below, we will find that the sub-seasonal WACE pattern related to the UB with the different phase of NAO can also have such meridional asymmetries during the PDO⁻ and AMO⁺ winters.

3.2. Meridional Asymmetry of Sub-Seasonal WACE Patterns Associated With UB Events

As noted in the above subsection, PDO⁻ and AMO⁺ favor the winter WACE pattern through the generation of sub-seasonal WACE patterns. Thus, it is worthwhile to further examine the meridional structure of the

LUO ET AL. 6 of 14

23284277, 2022, 1, Downloaded from https://sgupubs.onlinelibrary.wiley.com/doi/10.1029/2021EF002351 by Smy University At Albany, Wiley Online Library on [02/06/2023]. See the Terms and Conditions (https://onlinelibrary.wiley.com/terms-and-conditions) on Wiley Online Library for rules of use; OA articles are

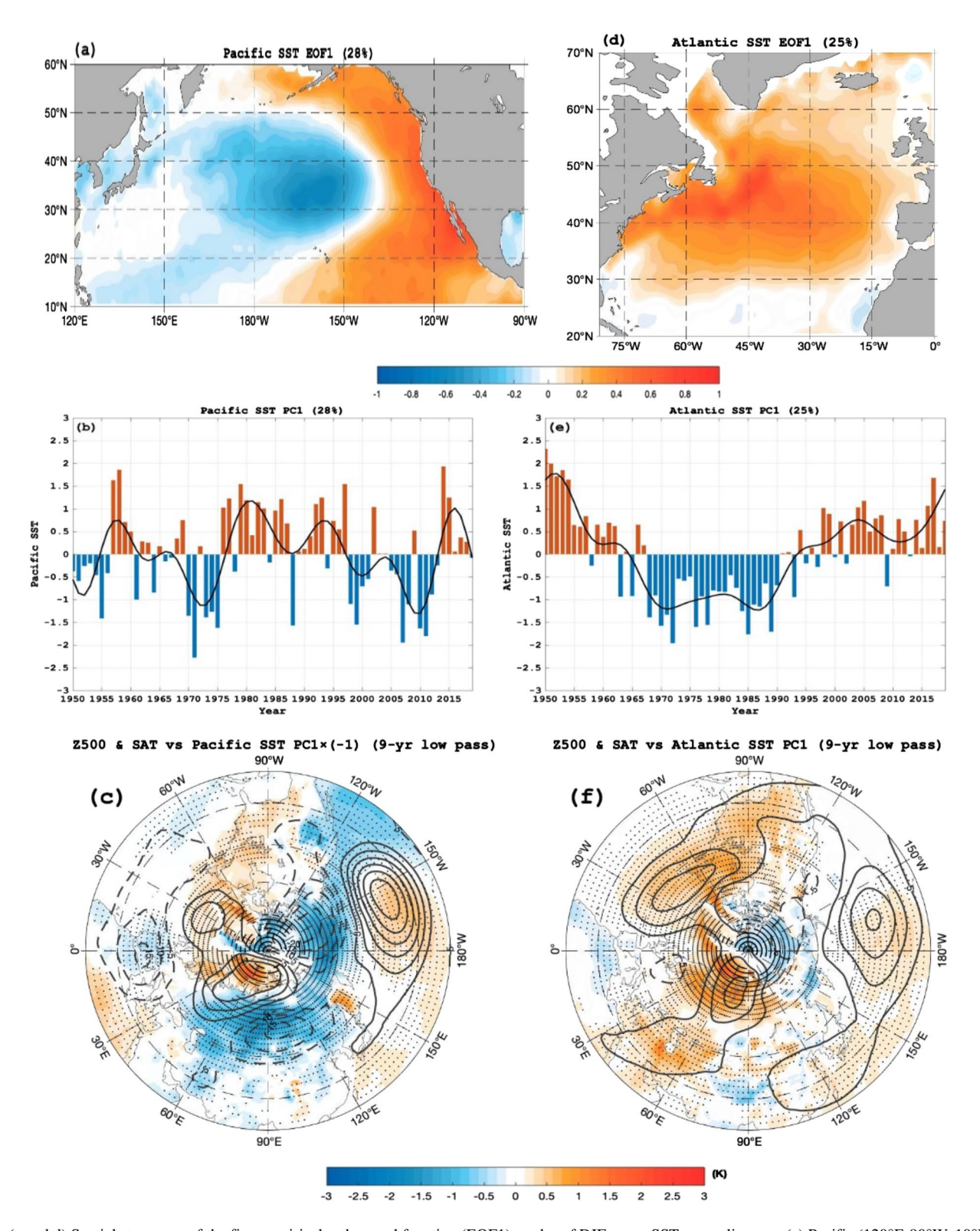


Figure 3. (a and d) Spatial structures of the first empirical orthogonal function (EOF1) modes of DJF-mean SST anomalies over (a) Pacific $(120^{\circ}E-90^{\circ}W, 10^{\circ}N-60^{\circ}N)$ and (d) North Atlantic $(80^{\circ}W-0, 20^{\circ}-70^{\circ}N)$ and (b and e) their corresponding normalized SST PC1 time series over (b) Pacific and (e) North Atlantic. (c and f) Regressed DJF-mean Z500 (contours, CI = 5 gpm STD⁻¹) and SAT (color shading in unit of K STD⁻¹) anomalies against the 9-yr low pass filtered normalized SST PC1 time series over (c) Pacific and (f) North Atlantic. The dot represents the shading region with a 95% confidence level based on a two-sided student t-test and the thick line in (b and e) denotes a 9-yr low pass curve.

LUO ET AL. 7 of 14

23284277, 2022, 1, Downloaded from https://agupubs.onlinelibrary.wiley.com/doi/10.1029/2021EF002351 by Suny University At Albany, Wiley Online Library on [02/06/2023]. See the Terms

and Conditions (https://onlinelibrary.wiley.com/terms-and-conditions) on Wiley Online Library for rule

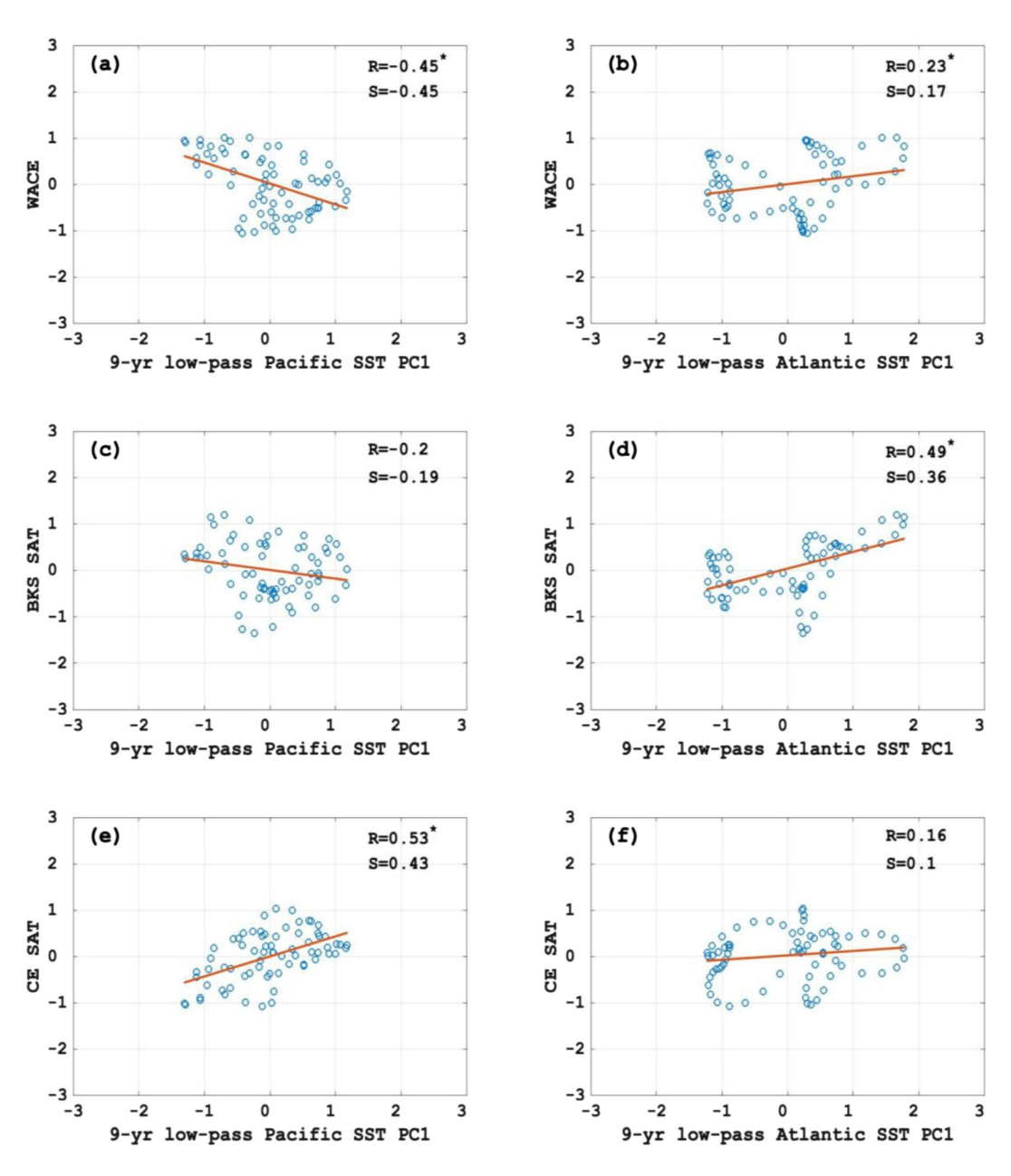


Figure 4. Scatter diagrams of normalized DJF-mean (a and b) WACE index and (c and d) BKS and (e and f) CE SAT time series against the normalized 9-yr low pass PC1 time series of the DJF-mean Pacific and Atlantic SST EOF1 modes, where the SAT anomaly over BKS (CE) are referred to as the BKS (CE) SAT. The value of R (S) denotes the correlation (slope) coefficient. A statistical significance with the 95% confidence level is marked by an asterisk.

sub-seasonal WACE pattern associated with UB events during the PDO⁻ and AMO⁺ winters. Here, we use the 9-year low-pass filtered Pacific (Atlantic) DJF-mean SST PC1 time series with <0 (>0) STDs to define PDO⁻ (AMO⁺) to guarantee that the sample size of the chosen PDO⁻ (AMO⁺) winters is enough large. In this case, there are 35 PDO⁻ (41 AMO⁺) winters during 1950-2019. We show the number of winter UB events in Figures 5a and 5b for PDO⁻ and AMO⁺, even though UB events could also occur in the PDO⁺ or AMO⁻ winter. Because PDO⁺ or AMO⁻ corresponds to cold Arctic-warm Eurasia (CAWE) patterns and UB events are short-lived during the CAWE winter (Kim et al., 2021), we do not examine the impact of PDO⁺ or AMO⁻ on UB events in this paper. It is further found that during 1950-2019 there are 58 (65) UB events for the PDO⁻ (AMO⁺) winter, corresponding to 1.66 (1.59) UB events per winter, indicating that PDO⁻ and AMO⁺ do not strongly influence the frequency of UB events, even though AMO and PDO modulate the evolution of UB in duration, intensity and movement via

LUO ET AL. 8 of 14

23284277, 2022, 1, Downloaded from https://agupubs.onlinelibrary.wiley.com/doi/10.1029/2021EF002351 by Suny University At Albany, Wiley Online Library on [02/06/2023]. See the Terms and Conditions (https://onlinelibrary.wiley.com/em/s-and-conditions) on Wiley Online Library for rules

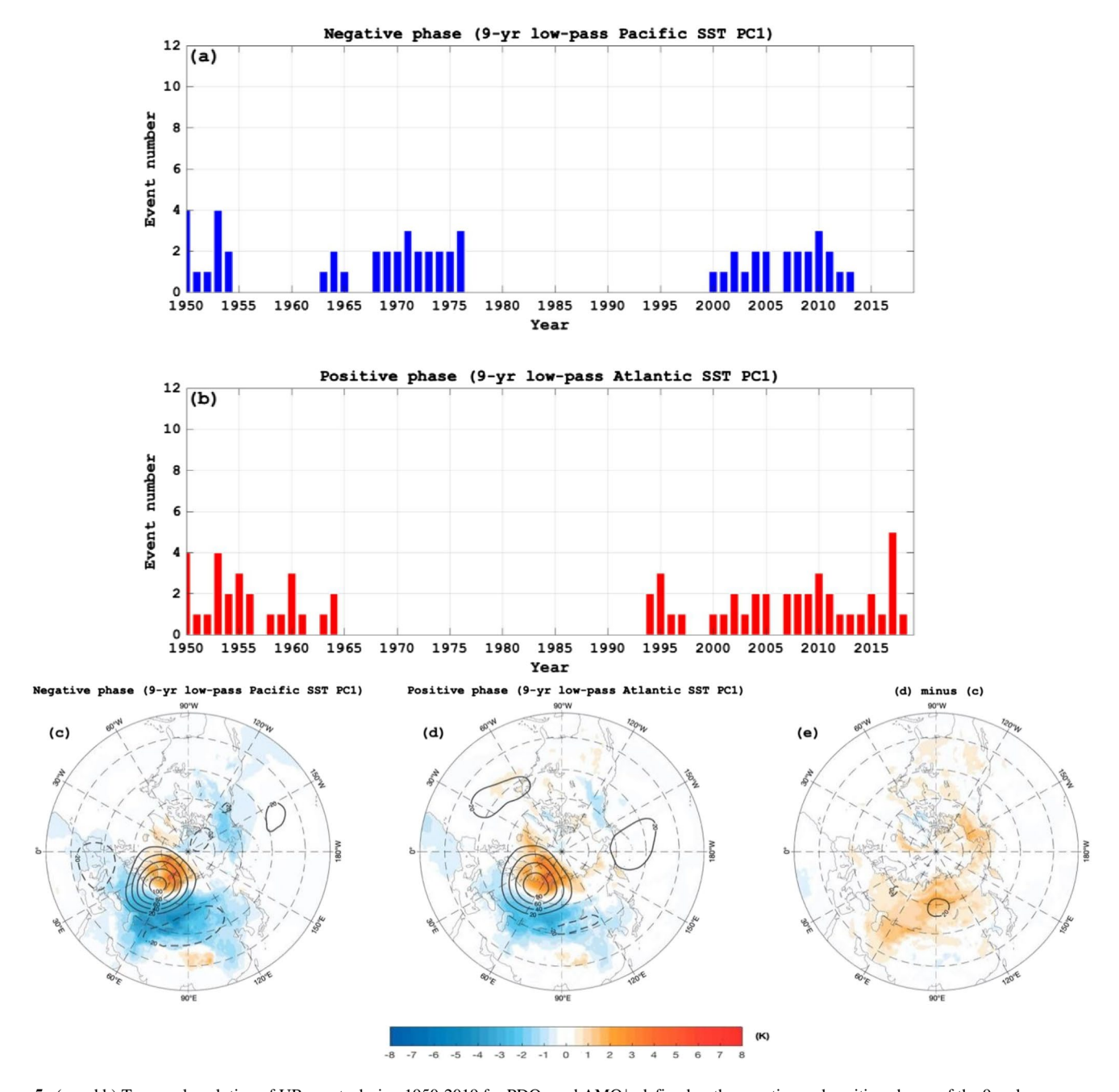


Figure 5. (a and b) Temporal evolution of UB events during 1950-2019 for PDO $^-$ and AMO $^+$, defined as the negative and positive phases of the 9-yr low pass normalized DJF-mean Pacific and Atlantic SST PC1 time series, respectively. (c and d) Time-mean fields of the composite daily Z500 (contours, CI = 20 gpm) and SAT (color shading, in K) anomalies averaged from lag -10 to +10 days of the UB events (lag 0 denotes the peak day of blocking) for (c) the negative phase of 9-yr low pass normalized Pacific SST PC1 time series (or PDO $^-$) and (d) the positive phase of 9-yr low pass normalized Atlantic SST PC1 time series (or AMO $^+$) and e their difference. The color shading represents the region with the SAT anomalies being significant with a 95% confidence level based on a two-sided student t-test, which is the same as below.

the change of meridional background potential vorticity gradient (D. Luo et al., 2019) (not shown). The less important impact of AMO and PDO on the frequency (event number) of UB events is easily explained because UB is not excited by PDO or AMO, instead it is mainly excited by the downstream propagation of sub-seasonal North Atlantic wave trains associated with the decay of NAO⁺ (Luo, Xiao, Yao, et al., 2016). The detailed discussions on the different effects of AMO and PDO on the evolution of UB will be reported in another paper.

LUO ET AL. 9 of 14

We show the time-mean field of composite daily Z500 and SAT anomalies averaged from lag –10 to 10 days (lag 0 denotes the peak day of blocking) of UB events in Figures 5c and 5d for PDO⁻ and AMO⁺ and their difference field in Figure 5e. It is interesting to see that the sub-seasonal WACE pattern associated with UB shows an asymmetric dipole structure with a weak warm anomaly over BKS and a strong cold anomaly over CE for PDO⁻ (Figure 5c). In contrast, the sub-seasonal WACE pattern during the UB episode shows a strong warm anomaly over BKS and a weak cold anomaly over CE in the AMO⁺ winter (Figure 5d). The difference between AMO⁺ and PDO⁻ can be clearly seen from Figure 5e. Thus, the meridional structures of the sub-seasonal WACE patterns are different between PDO⁻ and AMO⁺, which depend on whether PDO⁻ or AMO⁺ dominates. Naturally, a cumulative effect of strong sub-seasonal WACE events in winter leads to a strong winter WACE pattern with different meridional structures between PDO⁻ and AMO⁺. The meridional asymmetry of the WACE pattern and its physical cause were not mentioned in the previous studies (Chen et al., 2021; Jin et al., 2020; D. Luo et al., 2017; Sung et al., 2018).

3.3. Link of Sub-Seasonal WACE Patterns to the Different Phase of NAO Concurring With UB

The DJF-mean SAT anomaly not only depends on the turbulent heat fluxes (the sum of sensible and latent heat fluxes) associated with sea ice melting, but also on the downward infrared radiation associated with UB events under the different phases of NAO (B. Luo et al., 2017). Thus, it is useful to classify UB events to understand what type of UB events favor BKS warming under the modulation of PDO⁻ and AMO⁺. Our stratification reveals that there are 33 UB-NAO⁺, 14 UB-NAO⁻ and 11 UB-NAO^o events during the PDO⁻ winters, and 36 UB-NAO⁺, 14 UB-NAO^o and 15 UB-NAO^o events during the AMO⁺ winters. Their corresponding event numbers per winter are shown in Figure 6a for the negative (positive) phase of 9-year low pass normalized Pacific (Atlantic) SST PC1 time series. Clearly, most of UB events are linked to NAO⁺ even for PDO⁻ or AMO⁺. Namely, UB-NAO⁺ events are much more frequent than the other types of UB events. Luo, Xiao, Yao, et al. (2016) showed that most of UB events result from the decay or energy dispersion of sub-seasonal NAO⁺ driven by the North Atlantic storm track.

We show the time-mean composite daily Z500 and SAT anomalies averaged from lag -10 to 10 days of UB-NAO⁺, UB-NAO⁻ and UB-NAO^o events in Figures 6b, 6c, 6e, 6f, 6h and 6i for the negative (positive) value of 9-yr low pass normalized Pacific (Atlantic) SST PC1 time series and their differences in Figures 6d, 6g and 6j. It is noted that the sub-seasonal warm (cold) anomaly of composite UB-NAO+ events is stronger (weaker) for AMO+ (Figure 6c) than for PDO- (Figure 6b). Thus, AMO+ corresponds to a stronger sub-seasonal warming over BKS and Eurasian continent due to the effect of UB-NAO+ (Figure 6d) than PDO-. Although the Eurasian cold anomaly of the sub-seasonal WACE pattern associated with UB-NAO⁻ events shows a small difference between PDO⁻ (Figure 6e) and AMO⁺ (Figure 6f), the warm pole over the BKS is stronger for AMO⁺ (Figure 6f) than for PDO⁻ (Figure 6e); this is made very evident in their difference field shown in Figure 6g. One could hypothesize that the strong BKS warm anomaly during the UB-NAO episode is also related to warm Arctic water, strong sea ice melting and strong turbulent heat flux (the sum of downward sensible and latent heat fluxes) over BKS (Chen et al., 2018) during AMO⁺. However, for UB-NAO° events the Eurasian cold anomaly is stronger for PDO⁻ (Figure 6h) than for AMO⁺ (Figure 6i). Because UB-NAO⁺ events are much more frequent than other two types of UB events, the spatial structure of the sub-seasonal WACE pattern associated with UB events is mainly determined by UB-NAO+ events. This is a main reason of why the difference of the WACE pattern associated with UB-NAO⁺ events between AMO⁺ and PDO⁻ (Figure 6d) resembles that of UB events (Figure 5e). It is also found from Figures 6b and 6c that for the UB-NAO+ event the NAO+ is relatively weaker for PDO- (Figure 6b) than for AMO+ (Figure 6c). For this reason, the intrusion of North Atlantic midlatitude moisture into BKS via the UB-NAO+ relay (B. Luo et al., 2017) is also weaker for PDO- than for AMO+ (not shown). As a result, the UB-NAO+ leads to a weaker warming over BKS for PDO- (Figure 6b) than for AMO+ (Figure 6c) because of downward IR and downward turbulent heat flux over BKS being weaker during PDO- than during AMO+ (not shown). Such a process favors an asymmetric sub-seasonal WACE pattern.

4. Conclusion and Discussion

In this paper, we have examined the impact of PDO and AMO on the winter warm Arctic-cold Eurasia (WACE) pattern using seven decades of reanalysis data. It is found that the decadal variability of the WACE dipole pattern mainly results from the modulation of the PDO and AMO. While the negative PDO (PDO⁻) or positive AMO (AMO⁺) is favorable for the WACE pattern, the meridional asymmetry of the winter WACE dipole pattern is

LUO ET AL. 10 of 14

23284277, 2022, 1, Downloaded from https://agupubs.onlinelibrary.wiley.com/doi/10.1029/2021EF002351 by Suny University At Albany, Wiley Online Library on [02/06/2023]. See the Terms

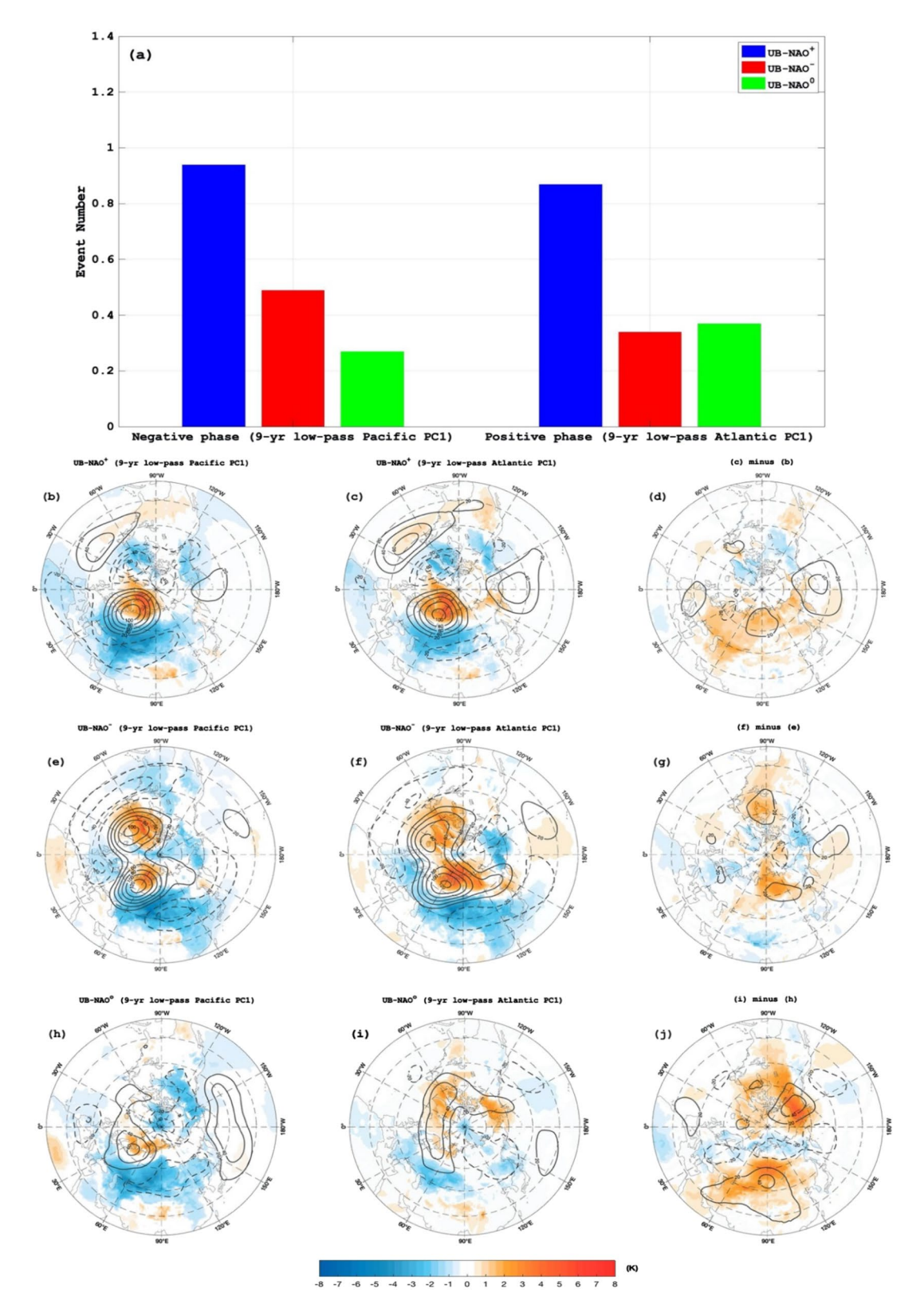


Figure 6. Histograms of UB-NAO⁺, UB-NAO⁻ and UB-NAO^o events per winter for (left) the negative phase of 9-yr low pass normalized Pacific SST PC1 time series and (right) the positive phase of 9-yr low pass normalized Atlantic SST PC1 time series. Time-mean composite daily Z500 (contours, CI = 10 gpm) and SAT (color shading, in K) anomalies averaged from lag -10 to 10 days of (b and c) UB-NAO⁺, (e and f) UB-NAO⁻ and (h and i) UB-NAO^o events for panel b, e, and h the negative phase of 9-yr low pass normalized Pacific SST PC1 time series and panel c, f and i the positive phase of 9-yr low pass normalized Atlantic SST PC as well as (d, g, j) their differences.

LUO ET AL. 11 of 14

23284277, 2022, 1, Downloaded

Wiley Online Library on [02/06/2023]. See the Term

mainly determined by whether PDO⁻ or AMO⁺ is dominant. The WACE pattern can have an asymmetric dipole structure with a weak warm anomaly over BKS and a strong cold anomaly over CE during the PDO⁻ winter. The relative strengths of the two poles of the WACE pattern are reversed in the AMO⁺ winters.

Daily compositing further shows that the winter WACE pattern is mainly related to sub-seasonal WACE patterns associated with UB events. The sub-seasonal WACE pattern can have a strong asymmetric dipole structure due to the modulation of PDO⁻ and AMO⁺. Because UB-NAO⁺ events are much more frequent than UB-NAO⁻ and UB-NAO⁺ events, the variability of the sub-seasonal WACE pattern is mainly related to UB-NAO⁺ events. While UB-NAO⁺ favors the intrusion of North Atlantic midlatitude moisture into Barents-Kara Seas (BKS) and increased tropospheric water vapor over BKS (B. Luo et al., 2017), the moisture intrusion and tropospheric water vapor are stronger during AMO⁺ than during PDO⁻ because NAO⁺ is weaker during PDO⁻ than during AMO⁺. As a result, a stronger BKS warming associated with stronger downward IR and turbulent heat flux (not shown) can be seen during AMO⁺ than during PDO⁻. Thus, an asymmetric sub-seasonal WACE pattern with strong (weak) warm anomaly over BKS and weak (strong) cold anomaly over CE is easily formed during the AMO⁺ (PDO⁻) winter, which can induce a strong meridional asymmetry of the winter WACE pattern.

It is worth noting that the combinations of the PDO⁻ and AMO⁺ have occurred during 2004-2019, when a positive WACE index occurs. It is difficult to distinguish the different roles of the PDO⁻ and AMO⁺ in the winter WACE pattern using this period alone. It should also be pointed out that the variability of the winter WACE pattern not only depends on the PDO and AMO on decadal-interdecadal timescales, but also on the ENSO and North Atlantic SST tripole pattern on interannual time scales. Although we have examined the impacts of the PDO and AMO on the winter WACE pattern based on the reanalysis data in this paper, the combined effects of ENSO with PDO or AMO on the winter WACE pattern are not explored here. These aspects warrant investigation, and will be explored in the future.

Data Availability Statement

The ERA5 reanalysis data from the website (https://climate.copernicus.eu/climate-reanalysis). The PDO and AMO indices are available online (http://climexp.knmi.nl/selectindex.cgi?id=someone@somewhere). The daily NAO index from (https://www.cpc.ncep.noaa.gov/products/precip/CWlink/pna/nao.shtml). The monthly SST data were taken from the website (https://www.metoffice.gov.uk/hadobs/index.html).

Acknowledgments

This research was supported by the National Natural Science Foundation of China (Grant number 41790473) and Chinese Academy of Sciences Strategic Priority Research Program (Grant XDA19070403).

References

Årthun, M., Eldevik, T., Smedsrud, L. H., Skagseth, Ø., & Ingvaldsen, R. B. (2012). Quantifying the influence of Atlantic heat on Barents Sea ice variability and retreat. *Journal of Climate*, 25, 4736–4743. https://doi.org/10.1175/JCLI-D-11-00466.1

Baldwin, M. P. & Dunkerton, T. J. (2001). Stratospheric harbingers of anomalous weather regimes. Science, 294, 581–584. https://doi.org/10.1126/science.1063315

Chen, X., Luo, D., Feldstein, S., & Lee, S. (2018). Impact of winter Ural blocking on Arctic sea ice: Short-time variability. *Journal of Climate*, 31, 2267–2282. https://doi.org/10.1175/jcli-d-17-0194.1

Chen, Y., Luo, D., & Zhong, L. (2021). North Atlantic interdecadal footprint of the recent warm Arctic-cold Siberia pattern. Climate Dynamics, 57, 121–139. https://doi.org/10.1007/s00382-021-05698-9

Chylek, P., Folland, C. K., Lesins, G., Dubey, M. K., & Wang, M. (2009). Arctic air temperature change amplification and the Atlantic Multidecadal Oscillation. Geophysical Research Letters, 36, L14801. https://doi.org/10.1029/2009GL038777

Cohen, J., Screen, J. A., Furtado, J. C., Barlow, M., Whittleston, D., Coumou, D., et al. (2014). Recent Arctic amplification and extreme mid-latitude weather. *Nature Geoscience*, 7, 627–637. https://doi.org/10.1038/ngeo2234

Dai, A. (2013). The influence of the inter-decadal Pacific oscillation on US precipitation during 1923–2010. Climate Dynamics, 41, 633–646. https://doi.org/10.1007/s00382-012-1446-5

Dai, A., Fyfe, J. C., Xie, S.-P., & Dai, X. (2015). Decadal modulation of global surface temperature by internal climate variability. *Nature Climate Change*, 5, 555–559. https://doi.org/10.1038/nclimate2605

Deser, C., Guo, R., & Lehner, F. (2017). The relative contributions of tropical Pacific sea surface temperatures and atmospheric internal variability to the recent global warming hiatus. *Geophysical Research Letters*, 44, 7945–7954. https://doi.org/10.1002/2017GL074273

Dong, B. & Dai, A. (2015). The influence of the Inter-decadal Pacific Oscillation on temperature and precipitation over the globe. Climate Dynamics, 45, 2667–2681. https://doi.org/10.1007/s00382-015-2500-x

Enfield, D. B., Mestas-Nuñez, A. M., & Trimble, P. J. (2001). The Atlantic multidecadal oscillation and its relation to rainfall and river flows in the continental. US Geophysical Research Letters, 28, 2077–2080. https://doi.org/10.1029/2000GL012745

Hersbach, H., Bell, B., Berrisford, P., Hirahara, S., Horányi, A., Muñoz-Sabater, J. (2020). The ERA5 global reanalysis. *Quarterly Journal of the Royal Meteorological Society*, 146, 1999–2049. https://doi.org/10.1002/qj.3803

Hu, D. & Guan, C. (2018). Decadal relationship between the stratospheric Arctic vortex and Pacific Decadal Oscillation. *Journal of Climate*, 31, 3371–3386. https://doi.org/10.1175/jcli-d-17-0266.1

LUO ET AL. 12 of 14

Earth's Future

23284277, 2022, 1, Downlo.

- Huang, J. P., Xie, Y. K., Guan, X. D., Li, D. D., & Ji, F. (2017). The dynamics of the warming hiatus over the Northern Hemisphere. Climate Dynamics, 48, 429–446. https://doi.org/10.1007/s00382-016-3085-8
- Jin, C., Wang, B., Yang, Y.-M., Yang, J., & Liu, J. (2020). Warm Arctic-cold Siberia as an internal mode instigated by North Atlantic warming. Geophysical Research Letters. 47, e2019GL086248. https://doi.org/10.1029/2019GL086248
- Kim, H.-J., Son, S.-W., Moon, W., Kug, J.-S., & Hwang, J. (2021). Subseasonal relationship between Arctic and Eurasian surface air temperature. Scientific Reports. 11, 4081. https://doi.org/10.1038/s41598-021-83486-5
- Kim, K. Y. & Son, S. W. (2016). Physical characteristics of Eurasian winter temperature variability. Environmental Research Letters, 11, 044009. https://doi.org/10.1088/1748-9326/11/4/044009
- Kug, J.-S., Jeong, J.-H., Jang, Y.-S., Kim, B.-M., Folland, C. K., Min, S.-K., & Son, S. W. (2015). Two distinct influences of Arctic warming on cold winters over North America and East Asia. Nature Geoscience, 8(10), 759–762. https://doi.org/10.1038/ngeo2517
- Lee, S., Gong, T., Feldstein, S. B., Screen, J. A., & Simmonds, I. (2017). Revisiting the cause of the 1989–2009 Arctic surface warming using the surface energy budget: Downward infrared radiation dominates the surface fluxes. *Geophysical Research Letters*, 44(20), 10654–10661. https://doi.org/10.1002/2017GL075375
- Li, C., Stevens, B., & Marotzke, J. (2015). Eurasian winter cooling in the warming hiatus of 1998–2012. Geophysical Research Letters, 42, 8131–8139. https://doi.org/10.1002/2015gl065327
- Li, M., Luo, D., Simmonds, I., Dai, A., Zhong, L., & Yao, Y. (2021). Anchoring of atmospheric teleconnection patterns by Arctic Sea ice loss and its link to winter cold anomalies in East Asia. *International Journal of Climatology*, 41, 547–558. https://doi.org/10.1002/joc.6637
- Liu, Z & Lorenzo, E. D. (2018). Mechanisms and predictability of Pacific Decadal variability. Current Climate Change Reports, 4, 128–144. https://doi.org/10.1007/s40641-018-0090-5
- Lu, Y., Tian, W., Zhang, J., Huang, J., Zhang, R., Wang, T., & Xu, M. (2021). The impact of the stratospheric polar vortex shift on the Arctic Oscillation. *Journal of Climate*, 34, 4129–4143. https://doi.org/10.1175/JCLI-D-20-0536.1
- Luo, B., Luo, D., Dai, A., Simmonds, I., & Wu, L. (2021). A connection of winter Eurasian cold anomaly to the modulation of Ural blocking by ENSO. Geophysical Research Letters, 48, e2021GL094304. https://doi.org/10.1029/2021GL094304
- Luo, B., Luo, D., Wu, L., Zhong, L., & Simmonds, I. (2017). Atmospheric circulation patterns which promote winter Arctic sea ice decline. Environmental Research Letters, 12, 054017. https://doi.org/10.1088/1748-9326/aa69d0
- Luo, B., Wu, L., Luo, D., Dai, A., & Simmonds, I. (2019). The winter midlatitude-Arctic interaction: Effects of North Atlantic SST and high-latitude blocking on Arctic sea ice and Eurasian cooling. Climate Dynamics, 52(5-6), 2981–3004. https://doi.org/10.1007/s00382-018-4301-5
- Luo, D., Chen, X., Overland, J., Simmonds, I., Wu, Y., & Zhang, P. (2019). Weakened potential vorticity barrier linked to recent winter Arctic sea ice loss and midlatitude cold extremes. *Journal of Climate*, 32, 4235–4261. https://doi.org/10.1175/jcli-d-18-0449.1
- Luo, D., Chen, Y., Dai, A., Mu, M., Zhang, R., & Simmonds, I. (2017). Winter Eurasian cooling linked with the Atlantic Multidecadal Oscillation.
- Environmental Research Letters, 12, 125002. https://doi.org/10.1088/1748-9326/aa8de8
 Luo, D., Xiao, Y., Diao, Y., Dai, A., Franzke, C. L. E., & Simmonds, I. (2016). Impact of Ural Blocking on winter Warm Arctic—Cold Eurasian
- anomalies. Part II: The link to the North Atlantic Oscillation. *Journal of Climate*, 29, 3949–3971. https://doi.org/10.1175/JCLI-D-15-0612.1 Luo, D., Xiao, Y., Yao, Y., Dai, A., Simmonds, I., & Franzke, C. L. E. (2016). Impact of Ural blocking on winter warm Arctic-cold Eurasian
- anomalies. Part I: Blocking induced amplification. *Journal of Climate*, 29, 3925–3947. https://doi.org/10.1175/JCLI-D-15-0611.1 Mantua, N. J., Hare, S. R., Zhang, Y., Wallace, J. M., & Francis, R. C. (1997). A Pacific interdecadal climate oscillation with impacts on
- salmon production. Bulletin of the American Meteorological Society, 78, 1069–1079. https://doi.org/10.1175/1520-0477(1997)078<1069: apicow>2.0.co;2
- McCusker, K. E., Fyfe, J. C., & Sigmond, M. (2016). Twenty-five winters of unexpected Eurasian cooling unlikely due to Arctic sea-ice loss. Nature Geoscience, 9(11), 838–842. https://doi.org/10.1038/ngeo2820
- Mori, M., Watanabe, M., Shiogama, H., Inoue, J., & Kimoto, M. (2014). Robust Arctic sea-ice influence on the frequent Eurasian cold winters in past decades. *Nature Geoscience*, 7, 869–873. https://doi.org/10.1038/ngeo2277
- Overland, J. E., Francis, J. A., Hall, R., Hanna, E., Kim, S.-J., & Vihma, T. (2015). The melting Arctic and mid-latitude weather patterns: Are they connected? *Journal of Climate*, 28, 7917–7932. https://doi.org/10.1175/jcli-d-14-00822.1
- Overland, J. E., Wood, K. R., & Wang, M. (2011). Warm Arctic-cold continents: Climate impacts of the newly open Arctic Sea. *Polar Research*, 30, 15787. https://doi.org/10.3402/polar.v30i0.15787
- Power, S., Casey, T., Folland, C., Colman, A., & Mehta, V. (1999). Inter-decadal modulation of the impact of ENSO on Australia. Climate Dynamics, 15, 319–324. https://doi.org/10.1007/s003820050284
- Qin, M., Dai, A., & Hua, W. (2020). Quantifying contributions of internal variability and external forcing to Atlantic multidecadal variability since 1870. Geophysical Research Letters, 47, e2020GL089504. https://doi.org/10.1029/2020GL089504
- Rayner, N. A., Parker, D. E., Horton, E. B., Folland, C. K., Alexander, L. V., Rowell, D. P., et al. (2003). Global analyses of sea surface temperature, sea ice, and night marine air temperature since the late nineteenth century. *Journal of Geophysical Research*, 108, 4407. https://doi.org/10.1029/2002JD002670
- Rudeva, I. & Simmonds, I. (2021). Midlatitude winter extreme temperature events and connections with anomalies in the Arctic and tropics. Journal of Climate, 34, 3733–3749. https://doi.org/10.1175/JCLI-D-20-0371.1
- Shepherd, T. (2016). Effects of a warming Arctic. Science, 353(6303), 989–990. https://doi.org/10.1126/science.aag2349
- Simmonds, I. & Li, M. (2021). Trends and variability in polar sea ice, global atmospheric circulations and baroclinicity. *Annals of the New York Academy of Sciences*, 1504, 167–186. https://doi.org/10.1111/nyas.14673
- Sun, L., Perlwitz, J., & Hoerling, M. (2016). What caused the recent "Warm Arctic, Cold Continents" trend pattern in winter temperatures? Geophysical Research Letters, 43, 5345–5352. https://doi.org/10.1002/2016gl069024
- Sung, M.-K., Kim, S.-H., Kim, B.-M., & Choi, Y.-S. (2018). Interdecadal variability of the Warm Arctic and Cold Eurasia Pattern and its North Atlantic origin. *Journal of Climate*, 31, 5793–5810. https://doi.org/10.1175/JCLI-D-17-0562.1
- Sutton, R. T., & Dong, B. (2012). Atlantic Ocean influence on a shift in European climate in the 1990s. *Nature Geoscience*, 5, 788–792. https://doi.org/10.1038/ngeo1595
- Tibaldi, S., & Molteni, F. (1990). On the operational predictability of blocking. *Tellus*, 42(3), 343–365. https://doi.org/10.1034/j.1600-0870.1990. t01-2-00003.x
- Trenberth, K. E., & Shea, D. J. (2006). Atlantic hurricanes and natural variability in 2005. Geophysical Research Letters, 33, L12704. https://doi.org/10.1029/2006GL026894
- Tyrlis, E., Bader, J., Manzini, E., Ukita, J., Nakamura, H., & Matei, D. (2020). On the role of Ural Blocking in driving the Warm Arctic-Cold Central Eurasia pattern. *Quarterly Journal of the Royal Meteorological Society*, 146, 2138–2153. https://doi.org/10.1002/qj.3784
- Wang, B., & An, S. I. (2005). A method for detecting season-dependent modes of climate variability: S-EOF analysis. Geophysical Research Letters, 32, L15710. https://doi.org/10.1029/2005GL022709

LUO ET AL. 13 of 14

23284277, 2022, 1, Downloaded from https:

doi/10.1029/2021EF002351 by Suny University At Albany, Wiley Online Library on [02/06/2023]. See the Terms

of use; OA articles are governed by the applicable Creative

- Wegmann, M., Orsolini, Y., & Zolina, O. (2018). Warm Arctic—cold Siberia: Comparing the recent and the early 20th-century Arctic warmings. Environmental Research Letters, 13, 025009. https://doi.org/10.1088/1748-9326/aaa0b7
- Wilks, D. S. (2011). Statistical methods in the atmospheric sciences (3rd Edition). Academic Press.
- Wyatt, M.G., Kravtsov, S., & Tsonis, A. A. (2012). Atlantic multidecadal Oscillation and Northern Hemispheres climate variability. *Climate Dynamics*, 38, 929–949. https://doi.org/10.1007/s00382-011-1071-8
- Xu, X., He, S., Li, F., & Wang, H. (2018). Impact of northern Eurasian snow cover in autumn on the warm Arctic-cold Eurasia pattern during the following January and its linkage to stationary planetary waves. Climate Dynamics, 50, 1432–0894. https://doi.org/10.1007/s00382-017-3732-8
- Yao, Y., Luo, D., Dai, A., & Simmonds, I. (2017). Increased quasi-stationarity and persistence of Ural blocking and Eurasian extreme cold events in response to Arctic warming. Part I: Insight from Observational Analyses. *Journal of Climate*, 30, 3549–3568. https://doi.org/10.1175/jcli-d-16-0261.1
- Ye, K. & Messori, G. (2020). Two leading modes of wintertime atmospheric circulation drive the recent warm Arctic—cold Eurasia temperature pattern. *Journal of Climate*, 33, 1520–0442. https://doi.org/10.1175/jcli-d-19-0403.1
- Zhong, L. H., Hua, L., & Luo, D. (2018). Local and external moisture sources for the Arctic warming over the Barents-Kara Seas. *Journal of Climate*, 31, 1963–1982. https://doi.org/10.1175/jcli-d-17-0203.1

LUO ET AL. 14 of 14